

No evidence for entrainment: endogenous gamma oscillations and rhythmic flicker responses coexist in visual cortex

Katharina Duecker^{1*}, Tjerk P. Gutteling¹, Christoph S. Herrmann², and Ole Jensen^{1*}

¹: University of Birmingham, School of Psychology, Centre for Human Brain Health, Birmingham, UK

²: Carl-von-Ossietzky University of Oldenburg, Faculty VI - Medicine and Health Sciences, Department of Psychology, Oldenburg, Germany

*Correspondence: kxd888@student.bham.ac.uk, o.jensen@bham.ac.uk

Abstract

Motivated by the plethora of studies associating gamma oscillations (~30-100 Hz) with various neuronal processes, including inter-regional communication and neuroprotection, we asked if endogenous gamma oscillations in the human brain can be entrained by rhythmic photic stimulation. The photic drive produced a robust Magnetoencephalography (MEG) response in visual cortex up to frequencies of about 80 Hz. Strong, endogenous gamma oscillations were induced using moving grating stimuli as repeatedly shown in previous research. When superimposing the flicker and the gratings, there was no evidence for phase or frequency entrainment of the endogenous gamma oscillations by the photic drive. Rather – as supported by source modelling – our results show that the flicker response and the endogenous gamma oscillations coexist and are generated by different neuronal populations in visual cortex. Our findings challenge the notion that neuronal entrainment by visual stimulation generalises to cortical gamma oscillations.

Key words: Magnetoencephalography; Neuronal Oscillations; Entrainment; Gamma Oscillations; Frequency Tagging; Flicker; Photic drive

Introduction

Neuronal cell assemblies have long been known to synchronise their discharges with millisecond precision (Buzsáki et al., 1992; Traub et al., 1996; Singer, 1999; Varela et al., 2001). This synchronisation has been linked to oscillatory activity in the gamma-frequency band (~ 30 -100 Hz) in various brain regions and species, e.g. in rodents and primates (e.g. Eckhorn et al., 1988; Gray & Singer, 1989; Engel et al., 1992; Wehr & Laurent, 1996; Brosch et al., 2002), including humans (e.g. Tallon et al., 1995; Müller et al., 1997; Rodriguez et al., 1999; Hoogenboom et al., 2006). Neuronal gamma oscillations have been proposed to support neuronal computations within populations (Singer & Gray, 1995; Singer, 1999; Von der Malsburg, 1999; Engel et al., 2001; Singer, 2009; Nikolić et al., 2013) as well as inter-regional functional connectivity through coherence (Bressler, 1990; Varela et al., 2001; Fries et al., 2007). Furthermore, they have been associated with various cognitive functions (see Başar-Eroglu et al., 1996; Herrmann & Mecklinger, 2001; Jensen et al., 2007; Tallon-Baudry, 2009; Uhlhaas et al., 2009, for review). In accordance with that, anomalies in gamma-band activity have been reported in neurological and psychological disorders that are related to impaired cognition and awareness, such as Autism Spectrum Disorder, Schizophrenia and Alzheimer's Dementia (see Herrmann & Demiralp, 2005; Uhlhaas & Singer, 2006; Uhlhaas et al., 2009; Traub & Whittington, 2010; Grützner et al., 2013, for review). In this study, we aimed to investigate if endogenous gamma oscillations in the human visual system can be driven non-invasively by rhythmic photic stimulation. Developing a methodology to directly manipulate gamma oscillations would allow to probe their role in neuronal processing and cognition, as well as their therapeutic potential. Indeed, in rodents, oscillatory neuronal responses to both optogenetics and a visual flicker at 40 Hz have been associated with neuroprotective responses and reduced neuroinflammation (Iaccarino et al., 2016; Adaikkan et al., 2019); making it a promising tool to reverse neurodegeneration linked to Alzheimer's Dementia. These findings have been explained by an *entrainment*, i.e. a synchronisation, of intrinsic gamma oscillations with the stimulation (Adaikkan & Tsai, 2020). The prerequisite of entrainment, as considered in dynamical systems theory, is the presence of a self-sustained oscillator that synchronises to the external drive (Pikovsky et al., 2003). This definition has often not been sufficiently embraced in studies of neuronal entrainment to sensory stimulation, as pointed out by Helfrich et al. (2019). A related phenomenon that is reflected by periodic responses to a rhythmic drive and an amplification of individually preferred rhythms is *resonance*

(Hutcheon & Yarom, 2000). Resonance does however not require the presence of self-sustained oscillations per se (Pikovsky et al., 2003; Helfrich et al., 2019). Indeed, oscillatory activity in response to a photic drive at frequencies ranging from 1 to up to 100 Hz in human Electroencephalography (EEG) recordings, have revealed a selective amplification of frequencies in the gamma band (Herrmann, 2001; Gulbinaite et al., 2019), indicating resonance in the visual cortex. Here, we explore both resonance and entrainment in the visual system to a visual flicker at frequencies >50 Hz. Stimulation at such high frequencies has recently been applied in Rapid Frequency Tagging (RFT) protocols, to investigate spatial attention (Zhigalov et al., 2019) and audiovisual integration in speech (Drijvers et al., 2020, bioRxiv), with minimal visibility of the flicker.

Oscillatory responses to photic stimulation from 52 to 90 Hz, recorded with MEG, were investigated in the presence and absence of visually induced gamma oscillations. In the *flicker* condition, the rhythmic drive was applied to a circular, invisible patch. In the *flicker&gratings* condition, the flicker was superimposed on moving grating stimuli that have been shown to reliably induce gamma oscillations (Hoogenboom et al., 2006, 2010; Van Pelt & Fries, 2013), thus meeting the precondition for entrainment. We expected the resonance properties of the visual system to change in presence of the endogenous gamma oscillations, as well as a synchronisation of the endogenous gamma oscillations with the rhythmic flicker. As we will demonstrate, the moving gratings did generate strong endogenous gamma oscillations, and the photic drive did produce robust responses at frequencies up to 80 Hz. However, to our great surprise, there was no evidence that the rhythmic stimulation entrains endogenous gamma oscillations.

Results

The aim of the current study was to characterise entrainment and resonance properties in the visual cortex in absence and presence of gamma-band oscillations induced by visual gratings. To this end, we drove the visual cortex with a rapid flicker at frequencies ranging from 52 to 90 Hz, in steps of 2 Hz. The photic drive was applied either to a circular patch (the *flicker* condition, Figure 10A,C) or to the light grey rings of a moving grating stimulus (the *flicker&gratings* condition, Figure 10B,D). We hypothesised that a photic drive within the frequency range close to the individual gamma frequency in the *flicker&gratings* condition would entrain the grating-induced oscillations. This would be observed as the endogenous gamma oscillation

synchronising with the drive. Moreover, we expected the presence of the induced gamma oscillator to change the resonance properties (compared to the *flicker* condition), reflected by an amplification of responses to stimulation frequencies equal or close to the endogenous gamma rhythm. Response magnitudes in the *flicker* condition were expected to reveal resonance properties of the visual system in absence of gamma oscillations, demonstrating favourable stimulation frequencies to be used in future experiments applying Rapid Frequency Tagging (RFT; Zhigalov et al., 2019; Drijvers et al., 2020).

Identifying Individual Gamma Frequencies

The frequency of the endogenous gamma rhythm is known to vary between participants (Hoogenboom et al., 2006, 2010; Muthukumaraswamy et al., 2010). Therefore, each subject's Individual Gamma Frequency (IGF) was identified first, based on the 0 - 2 s interval in the *flicker&gratings* condition during which the moving grating stimuli were presented without the visual flicker (Figure 10C). The Time-Frequency Representations (TFRs) of power are depicted in Figure 1A,B for two representative participants. The centre column shows the power averaged over time (0.25 - 1.75 s after the stimulus onset to avoid any event-related field confounds) demonstrating distinct peaks at 58 and 74 Hz for these participants. The topographies in the right column depict relative power change at the identified frequencies, focally in sensors over the occipital cortex. For each subject, the 2 - 3 combined planar gradiometers showing maximum relative power change in the gamma band were selected for further analysis (Sensors-of-Interest; SOI) per visual inspection. These sensors strongly overlapped between participants. The data of participants with an IGF closer than 6 Hz to the lowest (52 Hz) drive, i.e. $IGF < 58$ Hz, were not considered for further analyses.

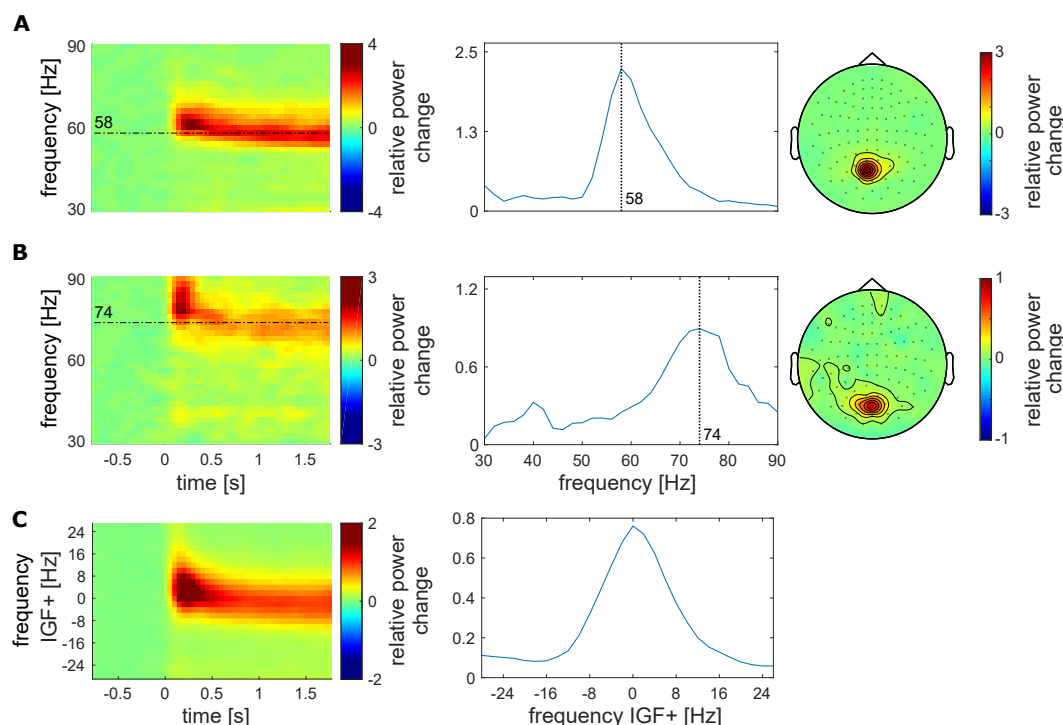


Figure 1: Identification of Individual Gamma Frequencies (IGF) and Sensors-of-Interest (SOI). **A, B** The TFRs of power, power spectra (averaged over 0.25 - 1.75 s) and topographic representations (combined planar gradiometers) of the IGF for two representative participants. The TFRs of power were calculated from the Fourier Transforms using a 500 ms sliding window, resulting in spectral smoothing of ± 3 Hz. The IGFs were identified from the spectral peak in 0.25 - 1.75s interval of the TFRs. Identified IGFs are indicated by dashed lines. **C** The grand-average of the power analysis after aligning the individual TFRs and spectra to the IGF (N=22).

Figure 1C depicts the averaged TFRs of power as well as the power spectrum for the remaining subjects (N=22), aligned to each participant's IGF prior to averaging. The moving grating stimulus induced sustained oscillatory activity constrained to the $\text{IGF} \pm 8$ Hz, with an average relative power change of 80% in the 0.25 - 1.75 s interval compared to baseline. In short, the moving gratings produced robust gamma oscillations observable in the individual participants which reliably allowed us to identify the individual gamma frequencies.

Photic drive induces responses up to ~80 Hz

We next set out to quantify the rhythmic response to the flicker as a function of frequency in the *flicker* condition, in which stimulation was applied to an invisible patch. Figure 2 A and B, left panel, depicts the overlaid power spectra for the different stimulation frequencies in two representative participants (the same as in Figure 1). The spectra were estimated by averaging the TFRs of power in the 0.25 - 1.75s interval after flicker onset. Due to the overlap of the sensors detecting the gamma oscillations and photic drive response (compare Figure 1 and 2 right columns) the same SOI were used as in the *flicker&gratings* condition. Both individuals showed strong responses at the respective stimulation frequencies, with a maximum relative power change of 200% and 500% in subject A and B, respectively. It should be noted that the IGFs (indicated by vertical dashed lines) did not relate to the frequencies where the strongest RFT signal occurred ($r(21) = 0.038$, $p = 0.87$, *flicker* condition). When averaged over all participants, the magnitude of the flicker response decreased systematically with frequency (Figure 2C).

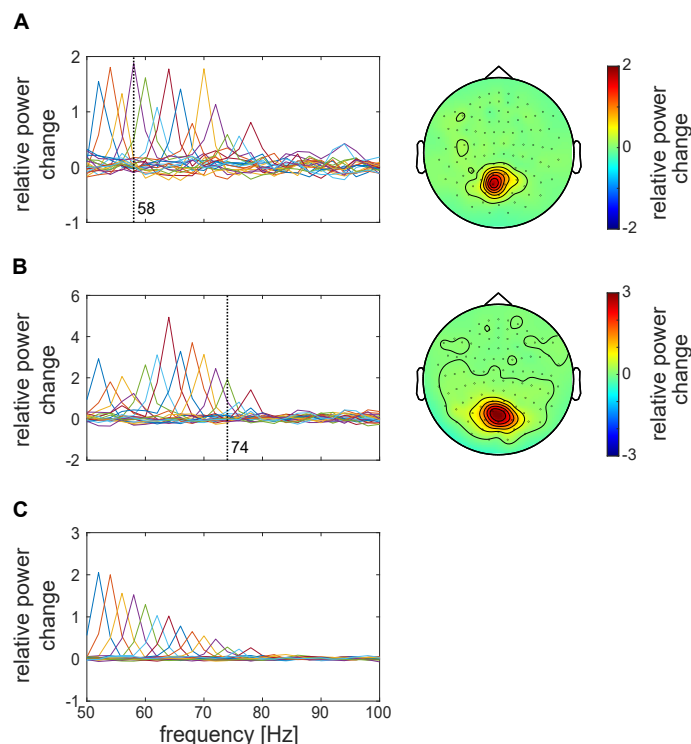


Figure 2: **A,B** The response to the photic drive in the *flicker* condition and the corresponding topographies for two representative subjects. Spectra were estimated from the TFRs of power averaged in the 0.25 - 1.75 s interval. Dashed vertical lines indicate the participants' IGF. The topographies (combined planar gradiometers) demonstrate a strong overlap with the ones in Figure 1. **C** Grand-average of the responses to the photic drive for each flicker frequency. On average, the magnitude of the flicker response decreases with increasing frequency, and is identifiable for stimulation below 80 Hz.

Figure 3A displays the power spectra in the *flicker* condition, estimated from the TFRs as explained above, averaged over all participants, as a function of stimulation frequency. These are equivalent to 2C. Diagonal values indicate the magnitude of the oscillatory responses (relative to baseline) at the stimulation frequencies, reaching values of up to 300% and decreasing monotonically with frequency. This confirms an upper limit for the stimulation of around 80 Hz. Off-diagonal values indicate oscillatory activity at frequencies different from the stimulation frequency. Figure 3B shows the same spectra after aligning to the individual IGFs, prior to averaging. Figure 3C and D display the spectra in the *flicker&gratings* condition

122 (averaged in the 2.25 - 3.75s interval), during which the photic drive was applied to the moving grating
 123 stimulus (see Figure 10B). The induced gamma band activity can be observed as the horizontal yellow band
 124 at ~ 60 Hz. When aligning the spectra to the IGF (Figure 3D), we observe a decrease in the flicker response
 125 but no evidence for an amplification at or close to the IGF.

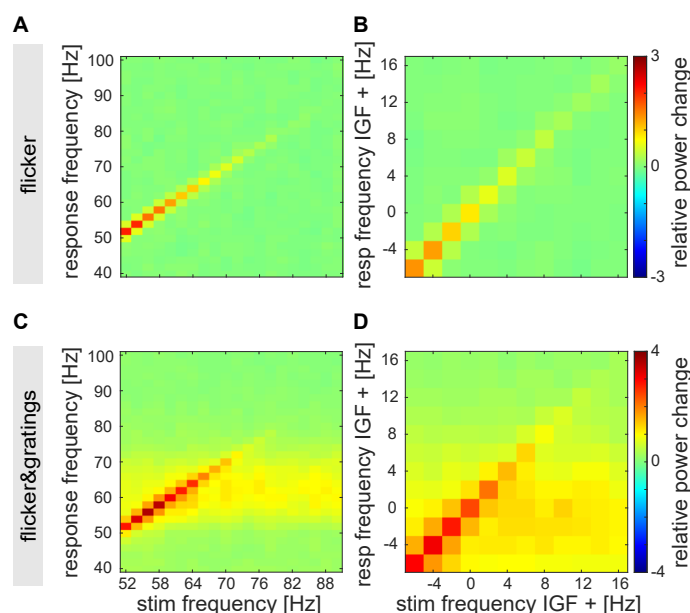


Figure 3: Average relative power change to the photic drive (y-axis) with respect to the driving frequencies (x-axis) **A** The *flicker* condition. Note that the power changes mirror Figure 2C. Power decreases with increasing frequency, from a relative change of ~ 3 at 52 HZ to $\sim .5$ at 80 Hz. **B** The *flicker* condition after the spectra were aligned to the IGF. **C** The *flicker&gratings* condition. All spectra demonstrate both the flicker response and induced gamma oscillation (observed as the yellow/orange horizontal band). Again, the amplitude of the rhythmic stimulation response appears to decrease with increasing frequency in both conditions. **D** The spectra for the *flicker&gratings* condition now aligned to the IGF. There is no indication that the rhythmic flicker captures the endogenous gamma oscillations.

126 **Magnitude of flicker response decreases as a function of frequency**

127 The averaged TFRs of power in Figure 3 point to an approximately linear decrease in power of the flicker
 128 response with increasing frequency. Literature on neural resonance and entrainment, however, suggests the

existence of a preferred rhythm at which oscillatory responses are amplified (Hutcheon & Yarom, 2000; Hermann, 2001; Pikovsky et al., 2003; Notbohm et al., 2016; Gulbinaite et al., 2019). As argued in Pikovsky et al. (2003) phase-locking between the driving signal and the self-sustained oscillator is the most appropriate metric to investigate entrainment. Figure 4A,B depicts the phase-locking value (PLV) between the photodiode and the MEG signal at the SOI (planar gradiometers, not combined). This measure reveals a systematic decrease in phase-locking with increasing flicker frequency for both the *flicker* (orange) and *flicker&gratings* (blue) condition (A). The observed relationship is preserved when aligning the frequencies to the IGF (B, also see Table 1). Note the absence of increased phase-locking at the IGF. The magnitude of the flicker response, quantified by power change compared to baseline, as a function of frequency, is demonstrated in Figure 4C-F and depicts a similar relationship to the one observed for the PLV. The *flicker* condition (C, orange line) revealed a systematic decrease with frequency, whereas the *flicker&gratings* condition did show a peak at 56 Hz. However, this observed increase appeared to be caused by considerable variance between the power estimates of the individual participants (see Figure 4E, each line graph depicts power estimates per individual participant). We again aligned the spectra to the IGF before computing the grand-average (Figure 4D). The absence of a peak at 0 Hz suggests no evidence for resonance at the IGF, confirming the peak at 56 Hz in C to be the result of inter-subject variability. Indeed, simple linear regression models, fit individually to PLV and power as a function of frequency aligned to the IGF, separately for each condition, explain a considerable amount of the variance (see Table 1 and dotted lines in Figure 4). We then identified the individual peak frequencies, eliciting the strongest response to the flicker in the *flicker&gratings* condition 4E, and related those to the IGF, as seen in Figure 4F. Importantly, the frequency inducing the strongest response to the rhythmic drive was below the IGF in the majority of participants, whereby the frequencies turned out to be uncorrelated ($r(21)=-0.15$, $p=0.5$, *flicker&gratings* condition).

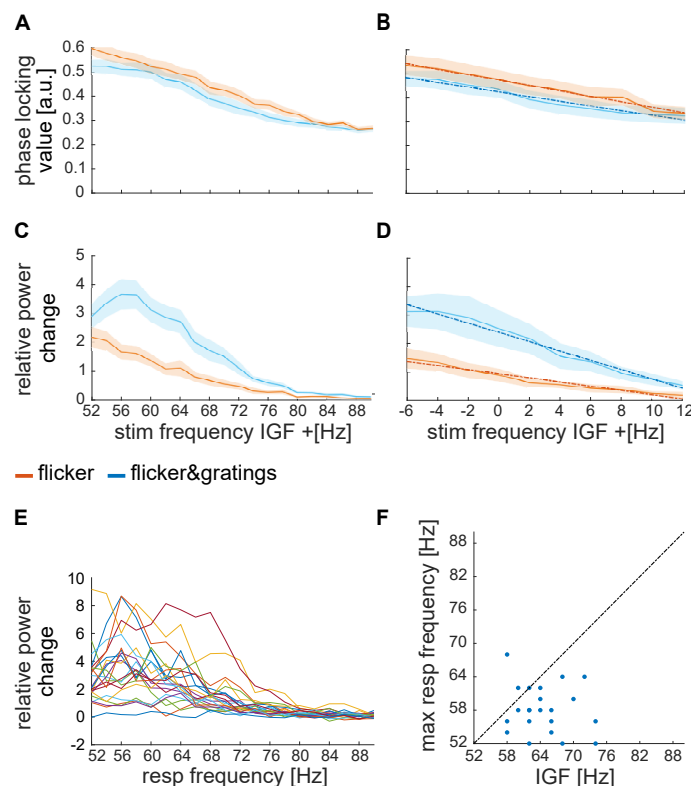


Figure 4: Magnitude of the flicker response as a function of frequency in the *flicker* (orange) and *flicker&gratings* (blue) condition. **A** The phase-locking values between the photo-diode and the MEG signal over the SOIs as a function of driving frequency. **B** The phase-locking values between the photo-diode and the MEG signals as a function of frequency after the spectra were aligned to IGF. Again, the phase-locking decreases with increasing frequency (see Table 1 for a statistical quantification of the simple linear regression models). **C** Relative power change with respect to baseline as a function of frequency. Generally, the power decreased with frequency, however, in the *flicker&gratings* there is an apparent peak at ~56 Hz; yet, the shaded errors (SE) indicate considerable variance between participants. **D** The relative power spectra as a function of frequency after the individual spectra were aligned in frequency according to the IGF, demonstrating that responses to a photic drive at the IGF are not amplified. **E** Relative power change as a function of frequency for each individual subject (N = 22), indicates that the peak at ~56 Hz in **C** is driven by comparably high power in that frequency range in just a few individuals. **F** Flicker frequency inducing highest power values versus IGF, demonstrating no systematic relationship ($r(21) = -0.15, p = .5$). Instead, the frequencies inducing maximum power change were below the IGF in the majority of participants⁴⁰

Table 1: Simple linear regression models: Flicker response magnitude as a function of distance to IGF.

Model	Estimates				
	β_1	t	p ***	R^2	F(1,218)
<i>flicker</i> _{plv}	-.01	-8.07	$< 2.2e - 16$.23	65.07
<i>flicker&gratings</i> _{plv}	-.01	-7.24	$< 2.2e - 16$.19	52.44
<i>flicker</i> _{pow}	-.07	-9.01	$4.80e - 14$.27	81.14
<i>flicker&gratings</i> _{pow}	-.16	-8.95	$7.51e - 12$.27	80.13

Gamma oscillations and flicker response coexist

We initially hypothesised that entrainment of the gamma oscillations in the *flicker&gratings* condition would result in the photic drive capturing the oscillatory dynamics when the driving frequency was close to endogenous gamma oscillations. Figure 5 depicts the TFRs of power relative to a 0.5 s baseline, for one representative subject (also shown in Figure 1 and 2A). The averaged trials for a photic drive at 52 Hz are shown in Figure 5A and separately for each flicker frequency in Figure 5B (Figure created using Kumpulainen, n.d.). The IGF (58 Hz for this subject) and the respective stimulation frequencies are indicated by dashed lines. The endogenous gamma oscillations, induced by the moving grating stimulus, are observed as the sustained power increase from 0 - 6 s whereas the flicker response is demonstrated by a power increase at 2 - 4 s. The plots reveal that gamma oscillations persist at the IGF and coexist with the response to the photic drive, which is particularly apparent for stimulation at 52 Hz (Figure 5 A). Furthermore, the power increase at the flicker frequency does not appear to outlast termination of the drive at $t = 4$ s. In the subsequent step, we frequency-aligned the TFRs of power according to the IGF before averaging over participants. Again, the analyses were constrained to individuals with an IGF above 56 Hz ($N = 22$).

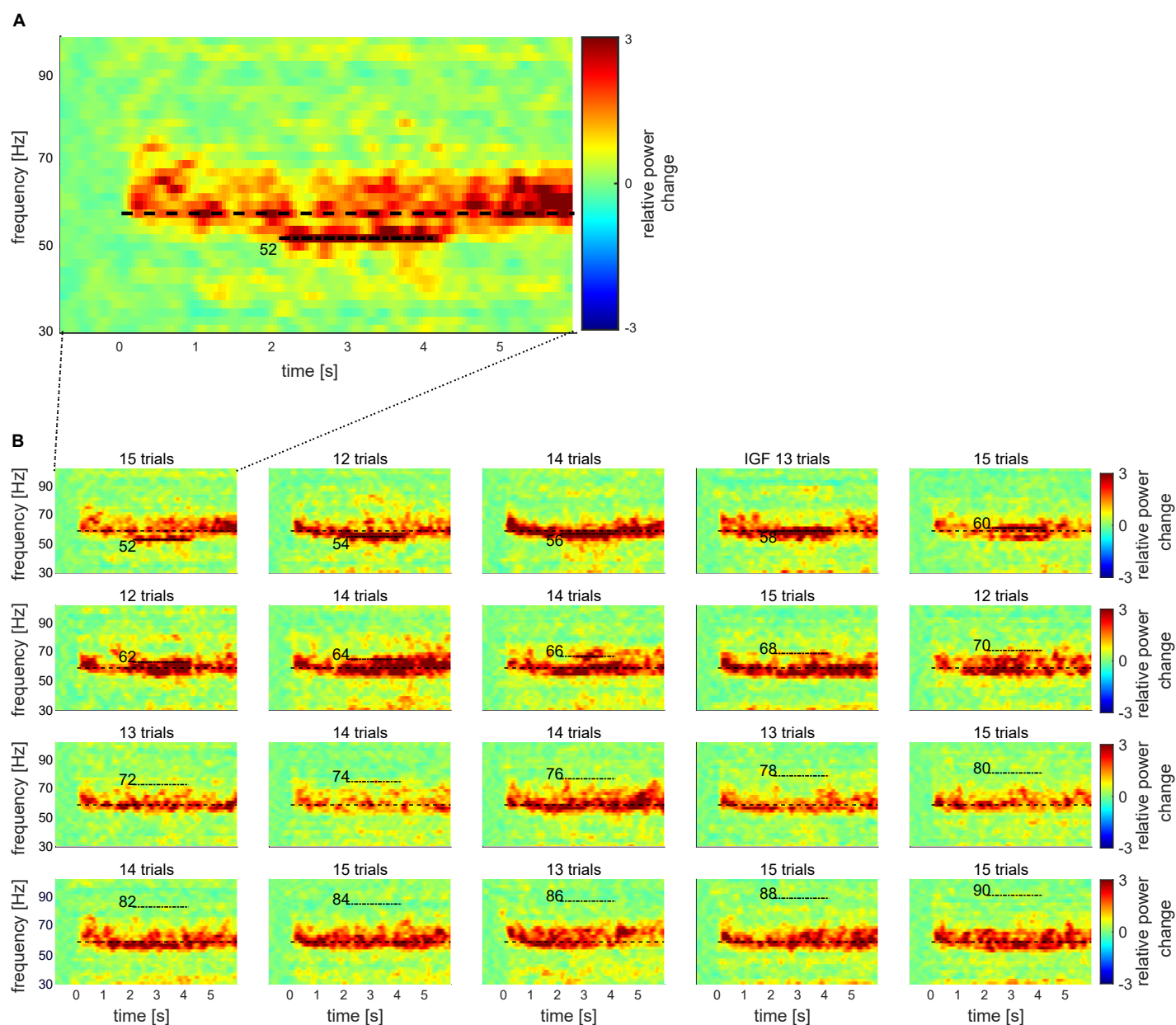


Figure 5: The time-frequency representations (TFRs) of power for one representative subject, showing relative power change averaged over trials and SOIs in the *flicker&gratings* condition. **A** Photic drive at 52 Hz. The moving grating stimuli were presented for 0 - 6 s whereas the flicker was applied from 2 to 4 s. Sustained gamma-band activity is clearly observable throughout the presentation of the stimuli, with a power increase of 3 relative to baseline. Additionally, the rhythmic stimulation elicited a response at 52 Hz, which seems to coexist with the gamma oscillations, indicating that the photic drive is unable to capture the dynamics of the gamma oscillation. **B** The plots for the frequencies from 52 to 90 Hz. Stimulation frequencies and IGF (here 58 Hz) are indicated by horizontal dashed lines. The flicker induced responses up to 66 Hz in this participant. Gamma oscillations persist in presence of flicker responses, suggesting that they coexist.

165 The group averaged, aligned TFRs are shown in Figure 6 for frequencies ranging from IGF-6 Hz to
166 IGF+16 Hz. The endogenous gamma oscillations are observed as the power increase extending from 0 - 6
167 s, and the flicker response as the power change in the 2 - 4 s interval marked by dashed lines, respectively.
168 The photic stimulation induces a reliable response that decreases toward 12 Hz above the IGF. Despite the
169 representation of the gamma oscillations being smoothed due to inter-individual differences, the averaged
170 aligned TFRs of power support the observations in the single subject data: both the gamma oscillations and
171 flicker response coexist in the 2 - 4 s interval. Furthermore, there is no indication of the gamma power being
172 reduced during RFT at frequencies close to, but different from, the IGF.

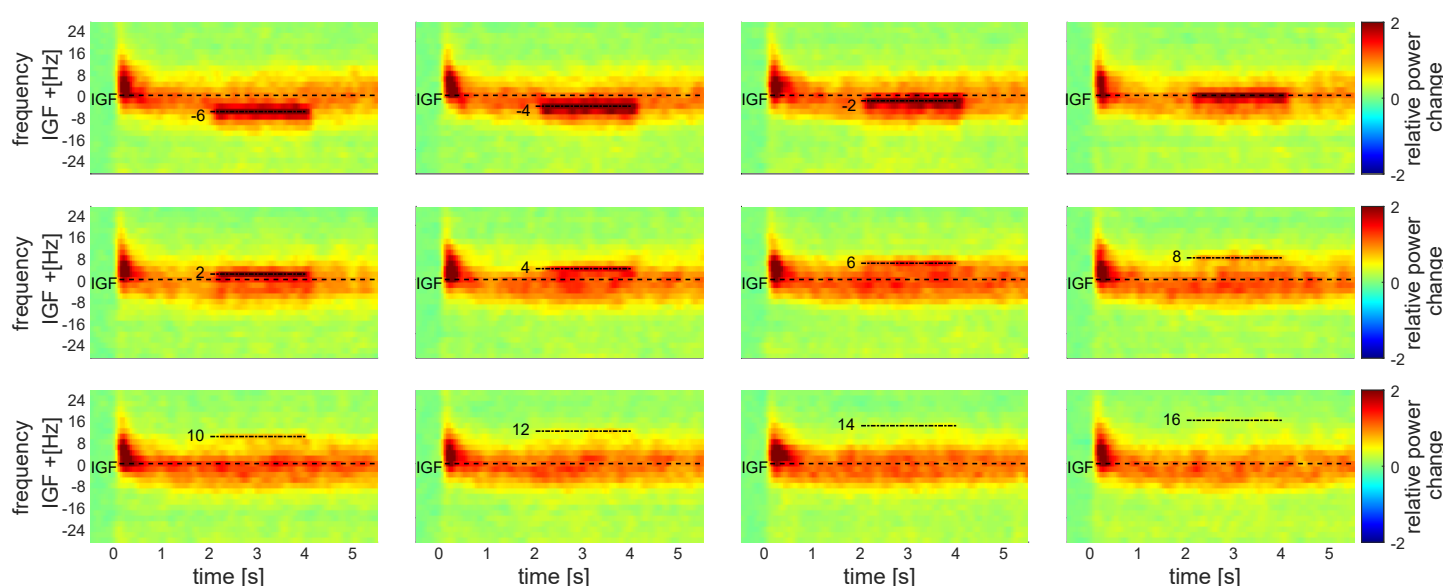


Figure 6: Grand-average TFRs of power after aligning to the IGF for each subject in the *flicker&gratings* condition. The stimulation frequencies (from -6 to 16 Hz relative to the IGF) are indicated by dashed horizontal lines. As suggested by the single subject TFRs in Figure 5, the endogenous gamma oscillations and the flicker response seem to be coexistent. Thus, there is no obvious indication of the photic drive being able to capture the dynamics of the gamma oscillations.

173 **No evidence that the oscillatory gamma dynamics can be captured by frequency entrainment**

174 Synchronisation of neuronal oscillations by rhythmic stimulation could be conceptualised as the entrainment
175 of a self-sustained oscillator by an external force (e.g. Notbohm et al., 2016; Helfrich et al., 2019). A central
176 assumption of this phenomenon is the existence of a 'synchronisation region' in the frequency range around
177 the endogenous frequency of the oscillator, the so-called Arnold tongue (e.g. Pikovsky et al., 2003). Driving
178 frequencies falling inside this synchronisation region, will be able to modulate the dynamics of the self-

sustained oscillator (also see Hutt et al., 2018). With this in mind, we investigated the power of the gamma oscillations before and during the photic drive for frequencies in the vicinity of the IGF (Figure 7) in the *flicker&gratings* condition. For each participant, we considered the relative power change induced by the moving gratings in the 0.5 - 1.5 s interval (T1) before the flicker onset and in the 2.5 - 3.5 s interval (T2) in which both the moving gratings and the photic drive were present. We investigated this for stimulation frequencies below the IGF (averaged power for -6 and -4 Hz) and above (averaged power for +4 and +6 Hz). Assuming a symmetric Arnold tongue centred at the IGF, as shown for entrainment in the alpha-band (Notbohm et al., 2016), we expected a reduction in power at the IGF in interval T2 for both higher and lower driving frequencies, i.e. an effect of time, but not frequency. Figure 7A depicts power change at the IGF for the factors stimulation frequency (drive<IGF and drive>IGF) and time interval (T1 and T2), averaged over the SOIs for each subject. In accordance with the TFRs in Figure 6, there is no meaningful indication for gamma power being reduced during the T2 interval as compared to the T1 interval, affirming the coexistence of the two responses. Surprisingly, power at the IGF seems to be slightly enhanced at T2 for drive>IGF. Indeed, a factorial repeated-measures ANOVA on the factors *time* and *frequency* did not reveal any significant main effects. However, there was a significant interaction effect of *interval* (T1 vs T2) and *frequency* (drive<IGF vs drive>IGF) ($F(1, 21) = 5.09, p = 0.003^{**}, \eta^2 = .003$), which was unexpected based on the assumption of a symmetrical synchronisation area around the IGF. A post-hoc dependent sample t-test, comparing power change at T2 relative to T1 for drive<IGF and drive>IGF (see Figure 7B) indicated that the interaction was driven by the increased gamma power during drive>IGF, $t(21) = -2.44, p = 0.012^*, 95\%CI = [-Inf - 0.029], r = .22$. Importantly, we were unable to find the expected reduction in gamma power during rhythmic photic stimulation, i.e. there was no indication that the rhythmic drive was capturing oscillatory gamma dynamics.

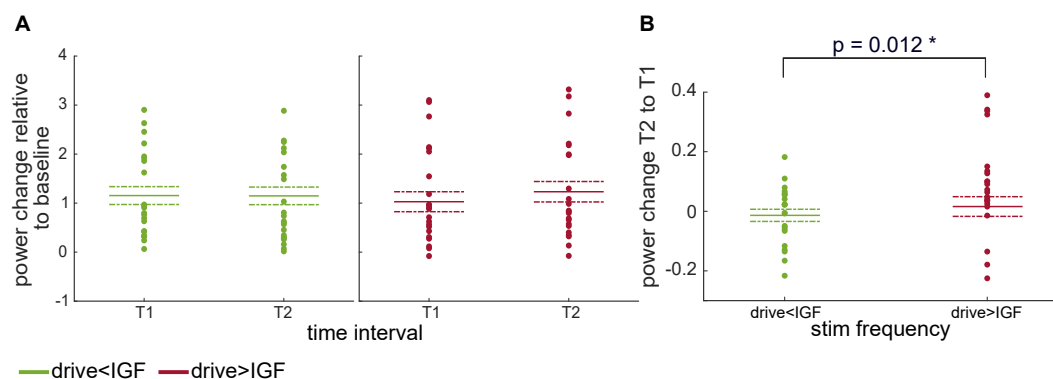


Figure 7: **A** Power change relative to baseline at IGF in response to the moving grating stimuli before (T1; 0.5 - 1.5 s) and during application of the flicker (T2; 2.5 - 3.5 s), at frequencies below and above IGF (drive<IGF [-6, -4 Hz] and drive>IGF [+4, +6 Hz], respectively). Scatters demonstrate individual values, solid and dashed lines depict mean and standard errors, respectively. The key finding is that power at T2 is not decreased compared to T1 for either of the frequency ranges. Instead, the plots show a slight increase in power at T2 for drive>IGF. A repeated measures ANOVA indicates a significant interaction of frequency and interval ($F(21, 1) = 5.09, p = 0.003^{**}, \eta^2 = .003$), but no main effect of time interval. **B** Power change at T2 relative to T1, for flicker frequencies below and above IGF. A post-hoc dependent sample t-test reveals that the interaction in **A** was driven by a significant increase of IGF power during the photic drive at frequencies just above IGF, ($t(21) = -2.44, p = 0.012^*, r = .22$).

Photic drive does not reliably modulate gamma phase

Synchronisation of a self-sustained oscillator by an external force, i.e. entrainment, is reflected by a constant phase angle between the two oscillators over extended intervals, so-called *phase plateaus*. These might occur when the frequency of the driver is close to the endogenous frequency of the oscillator, i.e. within its Arnold Tongue (Tass et al., 1998; Pikovsky et al., 2003; Notbohm et al., 2016). When approaching the edge of the synchronisation region, episodes of constant phase angles are interrupted by so-called *phase slips* that emerge when the self-sustained oscillator briefly unlocks from the driving force and oscillates at its own frequency. These phase slips will be observed as steps between the phase plateaus. We implemented the phase plateau analysis to complement the PLV analysis in Figure 4, which quantifies the average synchrony between photodiode and neuromagnetic signal over trials, but is not able to identify intermittent plateaus. If the photic drive entrains endogenous gamma oscillations, strong phase locking is expected, reflected by phase plateaus sustained over the duration of at least one cycle of the flicker frequency. These would be particularly pronounced during stimulation at and close to the IGF in the *flicker&gratings* condition, due to the

presence of the self-sustained gamma oscillator, but not in the *flicker* condition. To investigate phase entrainment of the gamma oscillations by the photic drive, we inspected the phase angle between the photodiode and one, individually selected, occipital gradiometer of interest per participant. Time series of phase per trial were estimated separately for the two signals, using a sliding time-window Fourier transform approach ($\Delta T = 3 \text{ cycles} = 3/f_{\text{flicker}} \text{ s}$; Hanning taper). Phase differences per trial were obtained by subtracting the unwrapped phase angle time series in the two sensors.

Phase angle between photodiode and MEG signal over time Figure 8 illustrates the unwrapped phase angles between the MEG and photodiode signal during the photic drive at the IGF (here 58 Hz), in the *flicker* (A) and *flicker&gratings* condition (B), respectively, for the same representative participant shown in Figure 1A, 2A and 5. Each coloured line graph depicts an individual trial. In both conditions, the MEG signal drifts apart from the photic drive, towards a maximum difference of 60 radians, i.e. a phase difference of about 9.5 cycles, by the end of the trial (A and B, top panel). Interestingly, the direction of the phase angle appears to change during some of the trials, suggesting spectral instability of the gamma oscillations. Furthermore, the graphs demonstrate a substantial inter-trial variability. This diffusion between trials, quantified for each participant as the standard deviation over trials at the end of the photic stimulation ($t=2$ in *flicker* and $t=4$ in *flicker&gratings* condition), converted from radiant to ms, is juxtapositioned in Figure 8C for the two conditions. It can be readily seen that the phase angles between the stimulation and MEG signal fan out highly similarly in absence and presence of the endogenous gamma oscillations.

Phase plateaus Visual inspection of the first 0.25 s of the phase angle times series, depicted in Figure 8A,B lower panel, does not suggest a comparably high number of phase plateaus in the *flicker&gratings* condition, that would have been expected if the photic drive was able to entrain the endogenous gamma oscillator. Importantly, the graphs demonstrate the phase angles to reach values of over 2π , i.e. more than one cycle, within the duration of the first gamma cycle (17.2 ms), suggesting that even stimulation at the endogenous frequency of the oscillator cannot capture the gamma dynamics. To verify these observations for the entire sample, plateaus during stimulation at the IGF were identified based on the mean absolute gradient (≤ 0.01 , see equation 3) over the duration of one cycle of stimulation, i.e. 18 consecutive samples for a flicker frequency of 58 Hz. Figure 8D shows the average number of plateaus per trial as a function of flicker

241 frequency aligned to IGF, averaged over participants. Again, the shaded areas indicate the standard error.
 242 While the *flicker&gratings* condition exhibits more phase plateaus than *flicker* for all stimulation frequen-
 243 cies, the number of plateaus decreases similarly in both conditions with increasing frequency. Importantly,
 244 stimulation at the IGF did not result in the highest number of plateaus in either condition. The results affirm
 245 the observations presented in Figure 4A and B.

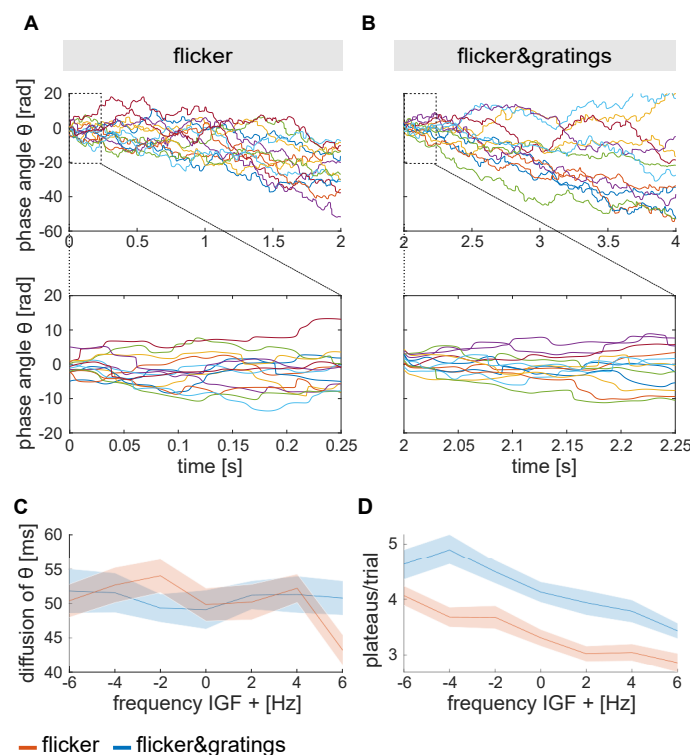


Figure 8: **A,B** Phase angle between photodiode and the MEG signal (one gradiometer of interest) at the IGF, for one representative participant; coloured lines depict individual trials. **A** Phase angle θ in the *flicker* condition over duration of the flicker presentation (upper panel) and the first 250 ms (lower panel). The MEG signal drifts apart from the stimulation and can reach a maximum accumulated phase difference of 60 rad, i.e. 9.54 cycles, at the end of the stimulation and up to 15 rad, i.e. 2.39 cycles, in 250 ms. **B** The increase in phase difference over the time of the stimulation for the *flicker&gratings* condition (upper panel) and in the first 250 ms (lower panel). The diffusion of the phase difference across trials is similar to the *flicker* condition. Moreover, there is no clear difference in the number and length of phase plateaus between conditions, implying that the presence of the gamma oscillations does not facilitate entrainment at the IGF. **C** Fanning out across trials as a function of frequency aligned to IGF. Trials diffuse to a highly similar extent in both conditions and across frequencies. **D** Number of plateaus per trial as a function of frequency. While the *flicker&gratings* conditions exhibits more plateaus for all flicker frequencies, there is no indication that stimulation at the IGF results in comparably strong synchronisation.

The sources of the gamma oscillations and the flicker response peak at different locations

The coexistence of the endogenous gamma oscillations and flicker response suggest that these two signals are generated by different neuronal populations; possibly in different regions. To test this assumption we localised the respective sources using Linearly Constrained Minimum Variance spatial filters (LCMV; Veen et al., 1992), estimated based on the data of the -0.75 to -0.25 baseline and the 0.25 to 1.75 s stimulation intervals in both conditions. Note that for each participant, one common filter was used for source estimation in both conditions. Power values at the IGF and flicker frequencies, averaged up to 78 Hz, respectively for the *flicker&gratings* and *flicker* condition, were extracted, and relative power change was computed at each of the 37,163 dipole locations using equation 1. Figure 9 illustrates the grand-average of the source localisation for the gamma oscillations (A) and flicker response (B). Consistent with previous work, both responses originate from mid-occipital regions (Hoogenboom et al., 2006; Zhigalov et al., 2019). Interestingly, the peak location of the endogenous gamma oscillator was significantly inferior to the flicker response (dependent sample t-test $t(21) = -5.12, p = 2.29e - 5^{***}, r = .55, 95\% CI = [-Inf - 5.67]$, see Figure 9C and D). Indeed, using the MNI to Talairach mapping online tool by Biomag Suite Web (MNI2TAL Tool) (see Lacadie et al., 2007, 2008), the centre peak of the gamma oscillations was located in the left secondary visual cortex (V2, Brodmann area 18; MNI coordinates = [-6mm -96mm -8mm]), while the peak of the flicker response was at a two millimetre distance to the primary visual cortex (V1, Brodmann area 17; MNI coordinates [6mm -96mm 4mm]). It should be noted, however, that using MRICroGL, with the Automated Anatomical Labelling atlas 3 (AAL3) (Rolls et al., 2020), the anatomical landmarks of the gamma oscillations and flicker responses were identified in the left and right Calcarine fissure (and surrounding cortex), respectively, which is considered to mainly cover the primary visual cortex (Johns, 2014). Crucially, while the sources of the gamma oscillations and the flicker response overlap to some extent, they peak in distinguishable locations in occipital regions.

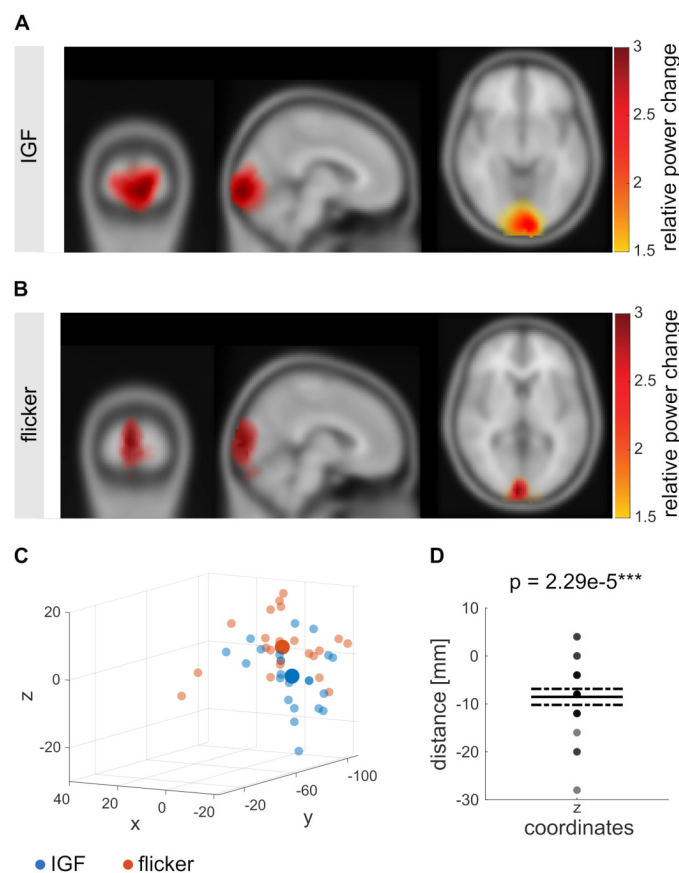


Figure 9: Source estimates using the LCMV beamformer approach mapped on a standardised MNI brain. **A** Source estimation of the visually induced gamma oscillations, with the peak of the source identified at MNI coordinates [0mm -98mm -7mm]. **B** Source estimation of the flicker response, with the average peak source at [3mm -96mm 2mm]. **C** Coordinates of the peak sources for all participants (small scatters) and grandaverage (large scatters) for the *flicker&gratings* and *flicker* condition (blue and orange, respectively), indicating that the gamma oscillations peak in brain areas inferior to the flicker response. **D** Difference between the z-coordinates (inferior-superior axis) of the peaks of the sources in both conditions, demonstrating an average difference of 8.5mm. A dependent sample t-test confirms this distance to be significant, $t(21) = -5.12, p = 2.29e - 5^{***}, r = .55, 95\% CI = [-Inf - 5.67]$.

Discussion

In this MEG study, we explored resonance properties and entrainment of the human visual system to a rapid photic drive >50 Hz in the absence and presence of endogenous gamma oscillations. Strong, sustained gamma oscillations were induced using moving grating stimuli (Hoogenboom et al., 2006, 2010; Van Pelt & Fries, 2013; Muthukumaraswamy & Singh, 2013). This allowed us to identify the individual gamma frequency in each participant. The photic drive induced responses for frequencies up to ~ 80 Hz, both in presence and absence of grating-induced endogenous gamma oscillations. To our surprise, we did not find evidence for resonance, i.e. an amplification of an individually preferred frequency in the range of the rhythmic stimulation, in either condition, despite the endogenous gamma rhythms being above 50 Hz in all participants. Moreover, there was no indication that the endogenous gamma oscillations synchronised with the rhythmic stimulation, i.e. no evidence for entrainment. Instead, the flicker response and the visually induced gamma-band activity appeared to coexist. Indeed, source estimation using Linearly Constrained Minimum Variance (LCMV) spatial filters (Veen et al., 1992), suggests that the neuronal sources of the flicker response and the endogenous gamma oscillations peak at distinct locations in visual cortex.

Endogenous gamma oscillations and flicker response might be generated by different populations

Low-pass filter properties of the visual system might hinder entrainment While the sources of the gamma oscillations and the response to the (nearly) invisible flicker did overlap in occipital cortex, their peak coordinates were found to be significantly different. Furthermore, the MNI2TAL online tool (see Lacadie et al., 2007, 2008) indicates that the two responses peak in different Brodmann areas, namely the primary (V1) and secondary visual cortex (V2), suggesting that the flicker response was unable to impact activity in visual cortex beyond V1. Several studies have considered the filter properties of different stages in the visual hierarchy of the mammalian brain (Cormack, 2005), i.e. retinal ganglion cells (e.g. Kuffler, 1953), lateral geniculate nucleus (LGN) of the thalamus and the primary visual cortex (e.g. Hawken et al., 1996; Carandini et al., 1997; Cormack, 2005; Ringach, 2004; Sharpee et al., 2006). The low-pass filter properties of the thalamus (Connelly et al., 2015) might have attenuated the photic drive in our data at frequencies above 80 Hz, leading to no measurable responses in this range. Interestingly, Hawken et al. (1996) found

low-pass filter properties at about 20 Hz in V1 in the projections from granular input layers (L4a, 4c α and 4c β) to supragranular (L2/3, 4b) and infragranular layers (L5,6) (also see Douglas & Martin, 2004; Fröhlich, 2016). Thus, the imposed flicker response might not travel beyond the granular layer of V1 and thus does not impact higher order visual areas, such as V2. This is supported by intracranial recordings in macaques which identified the strongest gamma synchronisation in response to drifting grating stimuli in V1 in supragranular layers (L2/3 and 4B) (Xing et al., 2012), whereas steady-state responses to a 60 Hz photic flicker were localised in granular layer 4c α (Williams et al., 2004).

Limitations of the source estimation It should be noted that the source localisation shown in Figure 9A and B represents an estimated location of the neuronal populations from which the two responses emerge. Moreover, while the neuromagnetic signal at locations inside the head can be estimated with a limited set of parameters (forward problem), there is no unique solution to describe the electromagnetic sources outside the skull (inverse problem) (Baillet, 2013). Therefore, interpretations of sources of neuromagnetic signals recorded with MEG should be interpreted tentatively. Also note that, besides the peak source, the localisation of the gamma oscillations also includes inferior and mid-occipital regions covering primary and secondary visual cortex. Indeed, in previous work, the origins of the grating-induced gamma oscillations have been found in both V1 and V2 (Hoogenboom et al., 2006, 2010, but see Buffalo et al. 2011; Roberts et al. 2013 for intra-cranial recordings in non-human primates). Again, it should be acknowledged that MRICroGL used with the AAL3 atlas (Rolls et al., 2020) indicates that both the gamma oscillations and flicker response emerge from Calcarine regions. Furthermore, due to the spectral width of the gamma oscillations (see Figure 1C), we were unable to localise the flicker response in the *flicker&gratings* condition without confounds with the endogenous oscillator. Despite the concerns outlined above, we found a systematic difference between the sources of the two oscillatory activities: the source of the gamma oscillations was found to be significantly inferior to the flicker response. Pairing the current paradigm with intracranial recordings in non-human primates would enable to test the reliability of this observation with higher spatial precision. Alternatively, computational models, as the one demonstrated by Lee & Jones (2013), would be suitable to investigate whether the grating-induced gamma oscillations and flicker response are likely to be generated by different neuronal populations.

No evidence for resonance at Individual Gamma Frequencies

Adaikkan et al. (2019) demonstrate compelling evidence for a visual flicker at 40 Hz to modulate neuronal responses, to strengthen synapses and to protect neurons and non-neuronal cells from degeneration, in rodents. These effects have been attributed to a synchronisation of endogenous gamma oscillations with the photic drive. In parallel to that, in human subjects, systematic analyses of steady-state responses to rhythmic flickering lights at a broad frequency range from 1-100 Hz (Herrmann, 2001) and 3-80 Hz (Gulbinaite et al., 2019) have revealed amplified responses to stimulation at ~ 40 and ~ 47 Hz. These findings at first suggest that oscillatory activity in the gamma-band can be driven by photic stimulation. However, while these studies demonstrate resonance properties of the human visual system in the lower gamma band, they do not demonstrate entrainment of endogenous oscillations. We hypothesised the resonance properties of the visual system to be particularly pronounced when endogenous gamma oscillation were induced, resulting in amplified responses to a photic drive at the IGF. Yet, we did not find evidence for the endogenous gamma oscillator to resonate to the photic drive. It is uncertain whether neuronal gamma oscillations in the human brain are more difficult to target with sensory stimulation than the rodent brain, e.g. due to differences in cell-type expressions, and their laminar distribution (Hodge et al., 2019). Alternatively, our findings might be specific to grating-induced gamma oscillations that have been shown to vary with size and contrast of the stimuli (Schadow et al., 2007; Muthukumaraswamy & Singh, 2013; Perry et al., 2013; Orekhova et al., 2015). Furthermore, it has been pointed out that such strong, narrow-band gamma oscillations are only reliably induced by gratings, but not all visual stimuli, suggesting that they are generated by specialised neuronal circuits (Hermes et al., 2015). It remains to be investigated whether our results generalise to gamma oscillations in different (and broader) frequency-bands that are associated with different functional properties (see Colgin et al., 2009; Ray & Maunsell, 2011; Buzsáki & Wang, 2012). Again, laminar recordings in non-human primates would allow conclusions about whether the neuronal populations receiving the photic input are able to converge to the neurons engaging in the endogenous gamma oscillations. Crucially, the results of the presented study imply that targeting endogenous gamma oscillations using sensory stimulation is not trivial.

Overlap of flicker and grating induced gamma oscillations

Gamma-band synchronisation in monkey area V4 has been shown to predict reaction times to a behaviourally relevant stimulus in a visual attention task (Womelsdorf et al., 2006). Similarly, in humans, both the gamma oscillations induced by a moving grating stimulus (Hoogenboom et al., 2010) and gamma-band flicker responses (F. Bauer et al., 2009) have been reported to accelerate target detection, suggesting them to tune and organise neuronal responses in a similar way. It remains to be identified whether these functionally and spectrally similar oscillations can be generated by distinct neuronal populations with no anatomical overlap. In that case, a rapid photic drive might not be feasible to probe the causal role of gamma oscillations, but it can be applied to modulate behaviour or for therapeutic purposes. Indeed, M. Bauer et al. (2012) have reported that while a 60 Hz influences drive perceptual processing, these effects appear to be independent of the stimulation phase; suggesting that they cannot be explained by an entrainment of endogenous oscillations.

Spectral precision of the individual gamma frequencies

The sliding time window approach paired with a 500ms Hanning taper, applied in the time-frequency analysis, induced spectral smoothing of ± 3 Hz. Consequently, the estimated IGFs are unlikely to perfectly match the true peak frequency of the endogenous gamma oscillator. Moreover, the stimulation frequencies were chosen to have a resolution of 2 Hz which further might result in the true gamma peak frequency being missed by the photic drive. Studies investigating entrainment in the alpha (Notbohm et al., 2016) and beta-band (Hanslmayr et al., 2014) in human subjects have demonstrated modulating effects on neuronal oscillations for stimulation rhythms within the range of the endogenous frequencies ± 1 Hz. Moreover, the natural peak of the identified gamma frequencies extends over a frequency range of about 10-16 Hz (IGF $\pm 5-8$ Hz), indicating that it should cover about 4 stimulation frequencies for each participant. Therefore, we conclude that the frequency resolution in this study does not explain the lacking evidence for entrainment. Our findings are contrasted by studies on visual entrainment of neuronal alpha oscillations (Schwab et al., 2006; Spaak et al., 2014; Notbohm et al., 2016; Fiene et al., 2020), which have been reported to emerge from infragranular (Spaak et al., 2012) as well as supragranular layers (Haegens et al., 2015; Dougherty et al., 2017). While our results do not support entrainment of oscillations in the gamma-band, these studies

show that it is indeed possible to entrain oscillations at lower frequencies.

Concluding remarks

Our results suggest that rapid photic stimulation does not entrain endogenous gamma oscillations and can therefore not be used as a tool to probe the causal role of gamma oscillations in cognition and perception. However, the approach can be applied in Rapid Frequency Tagging (RFT) to track neuronal responses without interfering, for instance, to investigate covert spatial attention (Zhigalov et al., 2019) and multisensory integration (Drijvers et al., 2020, bioRxiv).

Materials and Methods

Experiment

Experimental Procedure & Apparatus

The MEG data were recorded using a MEGIN Triux system housed in a magnetically shielded room (MSR; Vacuumschmelze GmbH & co., Hanau, Germany). Neuromagnetic signals were acquired from 204 orthogonal planar gradiometers and 102 magnetometers at 102 sensor positions. Horizontal and vertical EOG, the cardiac ECG signals, stimulus markers as well as luminance changes recorded by a photodiode (see below) were acquired together with the neuromagnetic signal. The data were lowpass filtered online at 330 Hz and sampled at 1000 Hz. Structural magnetic resonance images (MRIs), for later co-registration with the MEG data, were acquired using a 3 Tesla Siemens MAGNETOM Prisma whole-body scanner (Siemens AG, Muenchen, Germany), TE = 2 ms, and TR = 2 s). For two subjects, the T1-weighted images obtained in previous experiments, using a 3 Tesla Philips Achieva Scanner (Philips North America Corporation, Andover, USA), were used (scanned at the former Birmingham University Imaging Centre). Participants were invited to two separate sessions during which the MEG data and the anatomical images were acquired, respectively. Whenever possible, the MEG recording preceded the MRI scan; otherwise, the MEG session was scheduled at least 48 hours after the MRI session to avoid any residual magnetisation from the MRI system. Volunteers were requested to remove all metal items (e.g. jewellery) before entering the MSR. To enable later co-registration between MRI and MEG data, four to five head-position-indicator (HPI) coils were attached to the participants' foreheads. Along with the position of the coils, three fiducial landmarks

(nasion, left and right tragus) and over 200 head-shape samples were digitized using a Polhemus Fastrak (Polhemus, Colchester, USA). Following the preparations, the participants were seated in upright position under the dewar, with orientation set to 60°. The MEG experiment consisted of fifteen blocks lasting 4 min 30 s each. Participants were offered breaks every ~20 min but remained seated. At the beginning of each of these recording blocks, subjects were instructed to sit with the top and backside of their head touching the sensor helmet. The positions of the HPI coils relative to the sensors was gathered at the beginning of each recording block, but not continuously. The MEG experiment lasted ~75 min in total.

Rapid photic stimulation

Stimuli were presented using a Propixx lite projector (VPixx Technologies Inc, Saint-Bruno, QC Canada) which allows refresh rates of up to 1440 Hz. To achieve this high-frequency mode, the projector separates the screen (initial resolution: 1920 × 1080 pixels) into quadrants and treats them as separate frames, resulting in a display resolution of 960 × 540 pixels. The RGB colour codes for each quadrant, viz. red, green and blue, are converted to a greyscale, separately for each frame and colour, and presented consecutively within one refresh interval. The resulting twelve frames that are presented at a refresh rate of 120 Hz, i.e. 12 × 120 Hz = 1440 Hz. This approach allows to drive the luminance of each pixel with high temporal precision, allowing for smooth sinusoidal modulations, reducing unwanted harmonics (see Figure 10C,D). In this study, we applied rapid rhythmic stimulation at frequencies ranging from 52 to 90 Hz in 2 Hz increments.

Experimental Paradigm

Stimuli were created in MATLAB 2017a (The MathWorks, Inc. Natick, MA, USA) and presented using the Psychophysics Toolbox Version 3 (Brainard, 1997).

Conditions The experiment consisted of two conditions that will be referred to as the *flicker* and the *flicker&gratings* condition, respectively. Each trial began with a one-second interval, in which a central white fixation cross was presented on a dark grey background. In the *flicker* trials, a circular patch of size 6.47° was presented for 2 s. Its luminance was modulated sinusoidally at frequencies between 52 and 90 Hz (Figure 10A). Frequencies were randomised and balanced across trials. The patch was centred on the fixation cross, such that it was presented both foveally and parafoveally (Van Pelt & Fries, 2013, and see *Task & Time Course*). To minimise the visibility of the flicker, the mean luminance of the patch was matched

to the background (33% luminance, RGB [84 84 84]). Each trial ended with a two-second interval in which only the fixation cross was presented.

In the *flicker&gratings* condition, the baseline interval was followed by a 2 s presentation of a moving grating stimulus that has been shown to reliably elicit gamma oscillations in the visual cortex (e.g. Hoogenboom et al., 2006, 2010; Muthukumaraswamy & Singh, 2013; Tan et al., 2016). The stimulus was the same size as the patch (6.47°) and had a spatial frequency of 2.93 cycles/ $^\circ$ (see Figure 10B). The rings contracted towards the centre of the screen with a velocity of 1.06 $^\circ$ /s, i.e. 2.05 cycles/s. In the subsequent 2 s interval, the stimulus was flickered at the respective frequencies, followed by another 2 s interval in which the concentric moving circles remained on screen without photic stimulation. Note that the modulation of the luminance can only be applied to non-black tones and therefore only the grey rings of the grating were flickered. To keep the overall brightness of the stimulation similar between conditions, the luminance of the circular patch in the *flicker* condition ranged from 0 to 66% (of maximum luminance), while the brightness of the gratings in the *flicker&gratings* ranged from 33 and 99%. The flicker was applied to a small circular patch in the lower right corner of the screen, to acquire the stimulation signal with a photodiode.

Task & Time Course Participants were kept vigilant by performing a simple visual detection task that required them to respond to a 45° rotation of the fixation cross at the centre of the screen, which occurred once every minute (e.g. Zaehle et al., 2010). Data including the target and/or the responses were discarded and not considered in the analysis. The rotation took place after a trial in the majority, i.e. 60%, of the cases. The remaining 40% of rotations took place at any point during a trial. The experiment was divided into 15 blocks of 4.5 min, resulting in a recording time of 75 min in total. Within one block, each of the twenty stimulation frequencies were applied in both conditions, in randomised order. Thus, every block consisted of 40 frequency \times 2 condition combinations, resulting in a total of 15 repetitions of each of these combinations (i.e. 15 trials per flicker frequency for each of the two conditions). To minimise the amount of trials rejected by eye-blink artefacts, 3 s breaks, indicated by a motivating catchphrase or happy face on the screen, were incorporated every five trials, i.e. every 25 - 35 seconds. Participants were instructed to utilise these breaks to rest their eyes.

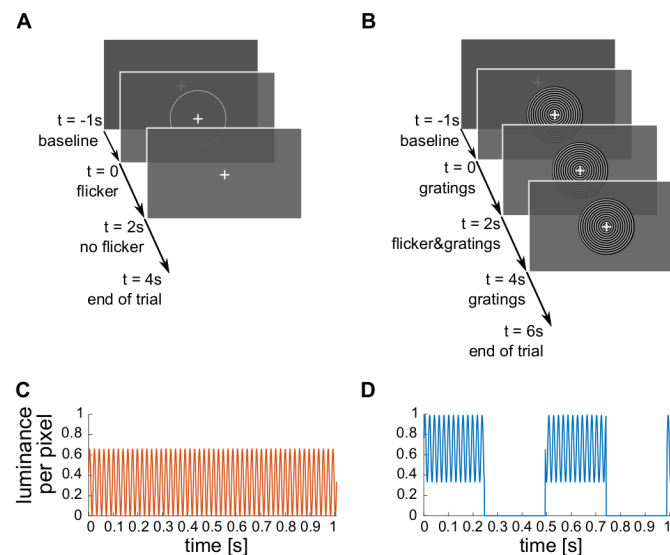


Figure 10: The experimental paradigm. **A** Trials in the *flicker* condition. A 1 s baseline interval with a central fixation cross was followed by a 2 s interval of the rapid flicker applied to circular patch of size 6.47° . The average luminance in the flickering patch was equal to the surrounding grey colour, making the flickering patch almost unperceivable. The trials ended with 2 s of the fixation cross only. **B** The trials in the *flicker&gratings* condition. The 1 s baseline interval was followed by 2 s of grating stimuli presented centrally on the screen, contracting inwards. Subsequently, the flicker was imposed onto the stimuli for 2 s. The trial ended with a 2 s presentation of the moving gratings without photic stimulation. **C** Sinusoidal luminance change in one pixel induced by the photic drive at 52 Hz in the *flicker* condition. **D** Luminance change in one pixel as a result of the flicker and the gratings moving concentrically with a velocity of 2.05 cycles/s. To maintain a similar mean luminance between conditions, photic modulation of the invisible patch in **A** ranged from 0 to 66% (mean RGB [84 84 84]), while the light grey rings of the grating, that is 50% of the stimulus' surface, were flickered between 33 and 99% (mean RGB [168 168 168] per ring).

455 Participants

456 This project was reviewed and approved by the local Ethics Committee at University of Birmingham, UK.

457 Thirty-one students of the University of Birmingham participated in the experiment. One experimental

session was terminated prematurely due to the participant not being cooperative, resulting in a sample of thirty participants (15 female), aged 25.7 ± 3.4 years. This sample size was decided upon based on a conceptually similar study investigating entrainment of neuronal alpha oscillations by Notbohm et al. (2016). All volunteers declared not to have had a history of neuropsychiatric or psychological disorder, reported to be medication-free and had normal or corrected-to-normal vision. For safety reasons, participants with metal items inside their bodies were excluded at the selection state. Prior to taking part in the study, participants gave informed consent, in accordance with the declaration of Helsinki, to both the MEG recording and the MRI scan and were explicitly apprised of their right to abort the experiment at any point. The reimbursement amounted to £15 per hour. To allow analysis of flicker responses at frequencies with a sufficient distance to the individual gamma frequency (IGF; see) of the participant, i.e. ± 6 Hz, 8 participants were excluded due to their IGF being below 58 Hz. Thus, the data of 22 participants were included in the following analyses (11 female; mean age 25.7 years).

Data Analysis

Analysis was performed in MATLAB 2017a and 2019b (The MathWorks, Inc. Natick, MA, USA) using the fieldtrip toolbox (Oostenveld et al., 2011).

Sensor Analysis

At the sensor level, the analysis was confined to the planar gradiometer signals, as these provided the best signal-to-noise ratio.

MEG preprocessing Trials containing the target or button presses were excluded. The data were read into MATLAB as 5 s and 7 s trials for the *flicker* and *flicker&gratings* conditions, respectively. Artefactual sensors were identified visually during and after the recordings for each participant, and interpolated with the data of their neighbouring sensors (0 to 2 sensors per participant). The individual trials were linearly detrended. Trials containing head movements and/or multiple eye blinks were discarded using a semi-automatic approach. An ICA approach ('runica' implemented in FieldTrip) was used to project out cardiac signals, eye blinks and eye movement. The sensor positions relative to the HPI coils were loaded in from the data files and averaged for each subject.

Time-Frequency Representation of Power Time-Frequency Representations (TFRs) of power were calculated using a sliding time-window approach ($\Delta T = 0.5$ s; 0.05 s steps). A Hanning taper (0.5 s) was applied prior to the Fourier-transform. This approach induced spectral smoothing of ± 3 Hz. Relative power change in response to the stimulation, i.e. the moving grating and/or the photic drive, was calculated as:

$$P_{\text{normalized}} = \frac{P_{\text{stim}}}{P_{\text{base}}} - 1 \quad (1)$$

with P_{stim} being the power during stimulation and P_{base} being the power in the baseline interval. The baseline interval was 0.75 - 0.25 s prior to the onset of the flicker (*flicker* condition) or the moving grating stimulus (*flicker&gratings* condition).

Individual Gamma Frequency The frequency band of the oscillatory activity elicited in response to the moving grating stimulus was identified individually per participant. TFRs of power were calculated for the baseline interval and presentation of the moving grating in the *flicker&gratings* condition and averaged over trials. The results were averaged over the 0.25 - 1.75 s interval, and the frequency bin with the maximum relative power was considered the Individual Gamma Frequency (IGF). In the case of two maxima, the average of the respective two frequencies was treated as the IGF. For each participant, the 4 to 6 gradiometers with the strongest gamma response to the moving gratings were selected as the Sensors-of-Interest (SOI).

Phase-Locking The average phase-synchrony between the photodiode (recording the visual flicker) and the neuromagnetic signal at the SOI was quantified by the Phase-Locking Value (PLV) (Lachaux et al., 1999; Bastos & Schoffelen, 2016) calculated using the 0.5 s sliding window multiplied with a Hanning taper of equal length. The phases of both signals were calculated from Fourier transformations, applied to the tapered segments. The PLV was computed separately for each *frequency* \times *condition*:

$$PLV = \frac{1}{n} \left| \sum_{n=1}^N \exp(j\theta(t, n)) \right| \quad (2)$$

where $\theta(t, n) = \phi_m(t, n) - \phi_p(t, n)$ is the phase difference between the MEG (m) and the photodiode (p) signal at time bin t in trial n (see Lachaux et al., 1999, p.195 and Figure 4 and 8).

Phase difference as a measure of entrainment Additionally, we investigated changes in phase difference between the photodiode and neuromagnetic signal over time for flicker frequencies of $IGF \pm 6$ Hz, to identify intervals of strong synchrony, so-called *phase plateaus*. MEG and photodiode signals ($\Delta T = 3$ cycles = $3/f_{flicker}$ s) were convolved with a complex Hanning taper using the sliding time window approach. Phase angles were derived from the Fourier transformed time series, unwrapped and subtracted to estimate the phase difference over time for each trial. Plateaus were defined as a constant phase angle (maximum average gradient 0.01 rad/ms) over the duration of one cycle of the stimulation frequency:

$$\frac{\sum_{i=1}^{\Delta T} |\nabla \theta_i|}{n} \leq 0.01 \text{ rad/ms} \quad (3)$$

with $\nabla \theta_i$ being the gradient, i.e. slope, of the phase angle between MEG and photodiode signal at a given sample i and n being the length of the cycle in ms, rounded up to the next integer, e.g. 17 ms for a flicker frequency of 60 Hz. While the PLV quantifies the average phase-similarity of the two signals over trials, this approach allows to investigate to what extent the stimulation and the MEG signal align in terms of phase-difference in a given time interval.

Statistical Analysis Statistical Analysis was performed in RStudio Version 1.2.1355 (RStudio Inc., Northern Ave, Boston, MA; R version 3.6.1., The R Foundation for Statistical Computing).

Source Analysis

MRI preprocessing The raw T1 weighted images were converted from DICOM to NIFTI. The coordinate system of the participants' individual MRI was aligned to the anatomical landmarks using the head-surface obtained from the MRI and the scalp shapes digitized prior to the recordings. Realignment was done automatically using the Iterative Closest Point (ICP) algorithm (Besl & McKay, 1992) implemented in the FieldTrip toolbox and corrected manually as necessary. The digitised headshape of one participant, for whom there was no anatomical image available, was aligned to a standardised template brain.

Linearly Constrained Minimum Variance Beamforming The neuroanatomical origins of the visually induced gamma oscillations in the *flicker&gratings* condition and the response induced by the photic drive in

the *flicker* condition were estimated using Linearly Constrained Minimum Variance spatial filters (LCMV; Veen et al., 1992), implemented in the Fieldtrip Toolbox (Oostenveld et al., 2011). The MEG forward model was calculated using single-shell head-models, estimated based on the aligned anatomical images, and an equally spaced 4-mm grid, warped into MNI (Montreal Neurologic Institute) space (Nolte 2003, also see Oostenveld et al., 2011; Stenroos et al., 2012); yielding 37,163 dipoles inside the brain. The pre-processed data, epoched in 7 and 5-second trials for the respective conditions, were band-pass filtered at 50 to 92 Hz, by applying second order Butterworth two-pass high- and low-pass filters. Segments of 0.5 s of the baseline interval (0.75 - 0.25 s prior to stimulation) and stimulation interval (0.75 - 1.25 s after flicker/grating onset) were derived from the filtered data. For each participant, a common covariance matrix for the 204 planar gradiometers was computed based on the extracted time series and used to estimate the spatial filter coefficients for each dipole location, whereby only the direction with the highest dipole moment was considered. Data in the baseline and stimulation intervals were projected to source space by multiplying each filter coefficient with the sensor time series. Fast Fourier Transforms of the resulting time series, multiplied with a Hanning taper, were computed for each of the 37,163 virtual channels, separately for the baseline and stimulation intervals, and averaged over trials. Relative power change at the IGF and flicker frequencies was computed by applying equation (1) to the Fourier-transformed baseline and stimulation intervals. The source-localised power change values at flicker frequencies up to 78 Hz were averaged to identify a common source for the oscillatory response to the photic drive.

Acknowledgements

This study was funded by a James S. McDonnell Foundation Understanding Human Cognition Collaborative Award (grant number 220020448), the Wellcome Trust Investigator Award in Science (grant number 207550), a BBSRC grant (BB/R018723/1), as well as the Royal Society Wolfson Research Merit Award (awarded to O.J.). The authors are grateful to Prof Veikko Jousmaki for providing the light-to-voltage converter and to Jonathan L. Winter, Nina Salman, Ludwig Barbaro, and Roya Jalali for help with the MEG recordings and MRI scans. The authors further thank Dr Simon Hanslmayr, Dr Geoffrey Brookshire and Dr Florian Kasten for feedback on the project and manuscript.

Conflict of interest statement: The authors declare no competing financial or non-financial interest.

Contributions: K.D., C.S.H. and O.J. conceptualised the study; K.D., T.P.G. and O.J. programmed the experiment; K.D. recorded the data; all authors analysed the data and wrote the manuscript.

References

- Adaikkan, C., Middleton, S. J., Marco, A., Pao, P. C., Mathys, H., Kim, D. N. W., ... Tsai, L. H. (2019). Gamma Entrainment Binds Higher-Order Brain Regions and Offers Neuroprotection. *Neuron*, 102, 929–943.e8. doi: 10.1016/j.neuron.2019.04.011
- Adaikkan, C., & Tsai, L. H. (2020). Gamma Entrainment: Impact on Neurocircuits, Glia, and Therapeutic Opportunities. *Trends in Neurosciences*, 43, 24–41. doi: 10.1016/j.tins.2019.11.001
- Baillet, S. (2013). Forward and Inverse Problems of MEG/EEG. In *Encyclopedia of Computational Neuroscience* (pp. 1–8). New York, NY: Springer New York. doi: 10.1007/978-1-4614-7320-6_529-1
- Bastos, A. M., & Schoffelen, J. M. (2016). A tutorial review of functional connectivity analysis methods and their interpretational pitfalls. *Frontiers in Systems Neuroscience*, 9, 175. doi: 10.3389/fnsys.2015.00175
- Bauer, F., Cheadle, S. W., Parton, A., Müller, H. J., & Usher, M. (2009). Gamma flicker triggers attentional selection without awareness. *Proceedings of the National Academy of Sciences of the United States of America*, 106, 1666–1671. doi: 10.1073/pnas.0810496106
- Bauer, M., Akam, T., Joseph, S., Freeman, E., & Driver, J. (2012). Does visual flicker phase at gamma frequency modulate neural signal propagation and stimulus selection? *Journal of Vision*, 12, 1–10. doi: 10.1167/12.4.5
- Başar-Eroglu, C., Strüber, D., Schürmann, M., Stadler, M., & Başar, E. (1996). Gamma-band responses in the brain: A short review of psychophysiological correlates and functional significance. *International Journal of Psychophysiology*, 24, 101–112. doi: 10.1016/S0167-8760(96)00051-7
- Besl, P. J., & McKay, N. D. (1992). A Method for Registration of 3-D Shapes. In *Ieee transactions on pattern analysis and machine intelligence* (Vol. 14, pp. 239–256). doi: 10.1109/34.121791
- Brainard, D. H. (1997). The Psychophysics Toolbox. *Spatial Vision*, 10, 433–436. doi: 10.1163/156856897X00357

580 Bressler, S. L. (1990). The gamma wave: a cortical information carrier? *Trends in Neurosciences*, 13,
581 161–162. doi: 10.1016/0166-2236(90)90039-D

582 Brosch, M., Budinger, E., & Scheich, H. (2002). Stimulus-related gamma oscillations in primate auditory
583 cortex. *Journal of Neurophysiology*, 87, 2715–2725. doi: 10.1152/jn.2002.87.6.2715

584 Buffalo, E. A., Fries, P., Landman, R., Buschman, T. J., & Desimone, R. (2011). Laminar differences in
585 gamma and alpha coherence in the ventral stream. *Proceedings of the National Academy of Sciences of*
586 *the United States of America*, 108, 11262–11267. doi: 10.1073/pnas.1011284108

587 Buzsáki, G., Horváth, Z., Urioste, R., Hetke, J., & Wise, K. (1992). High-frequency network oscillation in
588 the hippocampus. *Science*, 256, 1025–1027. doi: 10.1126/science.1589772

589 Buzsáki, G., & Wang, X. J. (2012). Mechanisms of gamma oscillations. *Annual Review of Neuroscience*,
590 35, 203–225. doi: 10.1146/annurev-neuro-062111-150444

591 Carandini, M., Heeger, D. J., & Movshon, J. A. (1997). Linearity and normalization in simple cells of the
592 macaque primary visual cortex. *Journal of Neuroscience*, 17, 8621–8644. doi: 10.1523/jneurosci.17-21
593 -08621.1997

594 Colgin, L. L., Denninger, T., Fyhn, M., Hafting, T., Bonnevie, T., Jensen, O., ... Moser, E. I. (2009).
595 Frequency of gamma oscillations routes flow of information in the hippocampus. *Nature*, 462, 353–357.
596 doi: 10.1038/nature08573

597 Connelly, W. M., Laing, M., Errington, A. C., & Crunelli, V. (2015). The thalamus as a low pass filter:
598 Filtering at the cellular level does not equate with filtering at the network level. *Frontiers in Neural*
599 *Circuits*, 9, 89. doi: 10.3389/fncir.2015.00089

600 Cormack, L. K. (2005). Computational Models of Early Human Vision. In *Handbook of image and video*
601 *processing* (pp. 325–345). Elsevier. doi: 10.1016/B978-012119792-6/50083-8

602 Dougherty, K., Cox, M. A., Ninomiya, T., Leopold, D. A., & Maier, A. (2017). Ongoing alpha activity in
603 V1 regulates visually driven spiking responses. *Cerebral Cortex*, 27, 1113–1124. doi: 10.1093/cercor/
604 bhv304

Douglas, R. J., & Martin, K. A. (2004). Neuronal circuits of the neocortex. *Annual Review of Neuroscience*, 27, 419–451. doi: 10.1146/annurev.neuro.27.070203.144152

Drijvers, L., Spaak, E., & Jensen, O. (2020). Rapid invisible frequency tagging reveals nonlinear integration of auditory and visual semantic information. *bioRxiv*. doi: 10.1101/2020.04.29.067454

Eckhorn, R., Bauer, R., Jordan, W., Brosch, M., Kruse, W., Munk, M., & Reitboeck, H. J. (1988). Coherent oscillations: A mechanism of feature linking in the visual cortex? - Multiple electrode and correlation analyses in the cat. *Biological Cybernetics*, 60, 121–130. doi: 10.1007/BF00202899

Engel, A. K., Fries, P., & Singer, W. (2001). Dynamic predictions: Oscillations and synchrony in top-down processing. *Nature Reviews Neuroscience*, 2, 704–716. doi: 10.1038/35094565

Engel, A. K., Konig, P., & Singer, W. (1992). Synchronization of oscillatory neuronal responses in cat striate cortex: Temporal properties. *Visual Neuroscience*, 8, 337–347. doi: 10.1017/S0952523800005071

Fiene, M., Schwab, B. C., Misselhorn, J., Herrmann, C. S., Schneider, T. R., & Engel, A. K. (2020). Phase-specific manipulation of rhythmic brain activity by transcranial alternating current stimulation. *Brain Stimulation*, 13, 1254–1262. doi: 10.1016/j.brs.2020.06.008

Fries, P., Nikolić, D., & Singer, W. (2007). The gamma cycle. *Trends in Neurosciences*, 30, 309–316. doi: 10.1016/j.tins.2007.05.005

Fröhlich, F. (2016). *Network Neuroscience*. Academic Press. doi: 10.1515/9781400851935-012

Gray, C. M., & Singer, W. (1989). Stimulus-specific neuronal oscillations in orientation columns of cat visual cortex. *Proceedings of the National Academy of Sciences of the United States of America*, 86, 1698–1702. doi: 10.1073/pnas.86.5.1698

Grützner, C., Wibrall, M., Sun, L., Rivolta, D., Singer, W., Maurer, K., & Uhlhaas, P. (2013). Deficits in high-(> 60 Hz) gamma-band oscillations during visual processing in schizophrenia. *Frontiers in Human Neuroscience*, 7, 88. doi: 10.3389/fnhum.2013.00088

Gulbinaite, R., Rooszendaal, D. H., & VanRullen, R. (2019). Attention differentially modulates the amplitude of resonance frequencies in the visual cortex. *NeuroImage*, 203, 116–146. doi: 10.1016/j.neuroimage

.2019.116146

Haegens, S., Barczak, A., Musacchia, G., Lipton, M. L., Mehta, A. D., Lakatos, P., & Schroeder, C. E. (2015). Laminar profile and physiology of the α rhythm in primary visual, auditory, and somatosensory regions of neocortex. *Journal of Neuroscience*, 35, 14341–14352. doi: 10.1523/JNEUROSCI.0600-15.2015

Hanslmayr, S., Matuschek, J., & Fellner, M. C. (2014). Entrainment of prefrontal beta oscillations induces an endogenous echo and impairs memory formation. *Current Biology*, 24, 904–909. doi: 10.1016/j.cub.2014.03.007

Hawken, M. J., Shapley, R. M., & Grosof, D. H. (1996). Temporal-frequency selectivity in monkey visual cortex. , 13, 477–492. doi: 10.1017/s0952523800008154

Helfrich, R. F., Breska, A., & Knight, R. T. (2019). Neural entrainment and network resonance in support of top-down guided attention. *Current Opinion in Psychology*, 29, 82–89. doi: 10.1016/j.copsyc.2018.12.016

Hermes, D., Miller, K., Wandell, B., & Winawer, J. (2015). Stimulus dependence of gamma oscillations in human visual cortex. *Cerebral Cortex*, 25, 2951–2959. doi: 10.1093/cercor/bhu091

Herrmann, C. S. (2001). Human EEG responses to 1-100 Hz flicker: Resonance phenomena in visual cortex and their potential correlation to cognitive phenomena. *Experimental Brain Research*, 137, 346–353. doi: 10.1007/s002210100682

Herrmann, C. S., & Demiralp, T. (2005). Human EEG gamma oscillations in neuropsychiatric disorders. *Clinical Neurophysiology*, 116, 2719–2733. doi: 10.1016/j.clinph.2005.07.007

Herrmann, C. S., & Mecklinger, A. (2001). Gamma activity in human EEG is related to highspeed memory comparisons during object selective attention. *Visual Cognition*, 8, 593–608. doi: 10.1080/13506280143000142

Hodge, R. D., Bakken, T. E., Miller, J. A., Smith, K. A., Barkan, E. R., Graybuck, L. T., ... Others (2019). Conserved cell types with divergent features in human versus mouse cortex. *Nature*, 573, 61–68. doi:

655 10.1038/s41586-019-1506-7

656 Hoogenboom, N., Schoffelen, J. M., Oostenveld, R., & Fries, P. (2010). Visually induced gamma-band
657 activity predicts speed of change detection in humans. *NeuroImage*, 51, 1162–1167. doi: 10.1016/
658 j.neuroimage.2010.03.041

659 Hoogenboom, N., Schoffelen, J. M., Oostenveld, R., Parkes, L. M., & Fries, P. (2006). Localizing human
660 visual gamma-band activity in frequency, time and space. *NeuroImage*, 29, 764–773. doi: 10.1016/
661 j.neuroimage.2005.08.043

662 Hutcheon, B., & Yarom, Y. (2000). Resonance, oscillation and the intrinsic frequency preferences of
663 neurons. *Trends in Neurosciences*, 23, 216–222. doi: 10.1016/S0166-2236(00)01547-2

664 Hutt, A., Griffiths, J. D., Herrmann, C. S., & Lefebvre, J. (2018). Effect of stimulation waveform on the
665 non-linear entrainment of cortical alpha oscillations. *Frontiers in Neuroscience*, 12, 376. doi: 10.3389/
666 fnins.2018.00376

667 Iaccarino, H. F., Singer, A. C., Martorell, A. J., Rudenko, A., Gao, F., Gillingham, T. Z., ... Tsai, L. H.
668 (2016). Gamma frequency entrainment attenuates amyloid load and modifies microglia. *Nature*, 540,
669 230–235. doi: 10.1038/nature20587

670 Jensen, O., Kaiser, J., & Lachaux, J. P. (2007). Human gamma-frequency oscillations associated with
671 attention and memory. *Trends in Neurosciences*, 30, 317–324. doi: 10.1016/j.tins.2007.05.001

672 Johns, P. (2014). *Clinical Neuroscience*. Elsevier Health Sciences. doi: 10.1016/c2009-0-35511-7

673 Kuffler, S. W. (1953). Discharge patterns and functional organization of mammalian retina. *Journal of*
674 *neurophysiology*, 16, 37–68. doi: 10.1152/jn.1953.16.1.37

675 Kumpulainen, P. (n.d.). Pekka Kumpulainen (2020). *tight_subplot(Nh, Nw, gap, marg_-*
676 *h, marg_w)* ([https://www.mathworks.com/matlabcentral/fileexchange/27991-tight_subplot-nh-nw-gap-](https://www.mathworks.com/matlabcentral/fileexchange/27991-tight_subplot-nh-nw-gap-marg_h-marg_w)
677 *marg_h-marg_w*), MATLAB Central File Exchange.

678 Lacadie, C. M., Fulbright, R. K., Arora, J., Constable, R. T., & Papademetris, X. (2007). Brodmann Areas
679 defined in MNI space using new Tracing Tool in BioImage Suite. In *Proceedings of the 14th annual*

meeting of the organization for human brain mapping (Vol. 36, p. 6494).

Lacadie, C. M., Fulbright, R. K., Rajeevan, N., Constable, R. T., & Papademetris, X. (2008). More accurate

Talairach coordinates for neuroimaging using non-linear registration. *NeuroImage*, 42, 717–725. doi:

10.1016/j.neuroimage.2008.04.240

Lachaux, J. P., Rodriguez, E., Martinerie, J., & Varela, F. J. (1999). Measuring phase synchrony in

brain signals. *Human Brain Mapping*, 8, 194–208. doi: 10.1002/(SICI)1097-0193(1999)8:4<194::

AID-HBM4>3.0.CO;2-C

Lee, S., & Jones, S. R. (2013). Distinguishing mechanisms of gamma frequency oscillations in human

current source signals using a computational model of a laminar neocortical network. *Frontiers in Human*

Neuroscience, 7, 869. doi: 10.3389/fnhum.2013.00869

Müller, M. M., Junghöfer, M., Elbert, T., & Rochstroh, B. (1997). Visually induced gamma-band responses

to coherent and incoherent motion: A replication study. *NeuroReport*, 8, 2575–2579. doi: 10.1097/

00001756-199707280-00031

Muthukumaraswamy, S. D., & Singh, K. D. (2013). Visual gamma oscillations: The effects of stimulus

type, visual field coverage and stimulus motion on MEG and EEG recordings. *NeuroImage*, 69, 223–230.

doi: 10.1016/j.neuroimage.2012.12.038

Muthukumaraswamy, S. D., Singh, K. D., Swettenham, J. B., & Jones, D. K. (2010). Visual gamma

oscillations and evoked responses: Variability, repeatability and structural MRI correlates. *NeuroImage*,

49, 3349–3357. doi: 10.1016/j.neuroimage.2009.11.045

Nikolić, D., Fries, P., & Singer, W. (2013). Gamma oscillations: Precise temporal coordination without a

metronome. *Trends in Cognitive Sciences*, 17, 54–55. doi: 10.1016/j.tics.2012.12.003

Nolte, G. (2003). The magnetic lead field theorem in the quasi-static approximation and its use for magne-

toencephalography forward calculation in realistic volume conductors. *Physics in Medicine and Biology*,

48, 3637–3652. doi: 10.1088/0031-9155/48/22/002

704 Notbohm, A., Kurths, J., & Herrmann, C. S. (2016). Modification of brain oscillations via rhythmic light
705 stimulation provides evidence for entrainment but not for superposition of event-related responses. *Frontiers in Human Neuroscience*, 10, 10. doi: 10.3389/fnhum.2016.00010

707 Oostenveld, R., Fries, P., Maris, E., & Schoffelen, J. M. (2011). FieldTrip: Open source software for
708 advanced analysis of MEG, EEG, and invasive electrophysiological data. *Computational Intelligence and*
709 *Neuroscience*, 2011, 115678–156869. doi: 10.1155/2011/156869

710 Orekhova, E. V., Butorina, A. V., Sysoeva, O. V., Prokofyev, A. O., Nikolaeva, A. Y., & Stroganova, T. A.
711 (2015). Frequency of gamma oscillations in humans is modulated by velocity of visual motion. *Journal*
712 *of Neurophysiology*, 114, 244–255. doi: 10.1152/jn.00232.2015

713 Perry, G., Hamandi, K., Brindley, L. M., Muthukumaraswamy, S. D., & Singh, K. D. (2013). The properties
714 of induced gamma oscillations in human visual cortex show individual variability in their dependence on
715 stimulus size. *NeuroImage*, 68, 83–92. doi: 10.1016/j.neuroimage.2012.11.043

716 Pikovsky, A., Kurths, J., Rosenblum, M., & Kurths, J. (2003). *Synchronization: a universal concept in*
717 *nonlinear sciences* (Vol. 12). USA: Cambridge University Press.

718 Ray, S., & Maunsell, J. H. (2011). Different origins of gamma rhythm and high-gamma activity in macaque
719 visual cortex. *PLoS Biology*, 9. doi: 10.1371/journal.pbio.1000610

720 Ringach, D. L. (2004). Mapping receptive fields in primary visual cortex. *Journal of Physiology*, 558,
721 717–728. doi: 10.1113/jphysiol.2004.065771

722 Roberts, M. J., Lowet, E., Brunet, N. M., TerWal, M., Tiesinga, P., Fries, P., & DeWeerd, P. (2013). Robust
723 gamma coherence between macaque V1 and V2 by dynamic frequency matching. *Neuron*, 78, 523–536.
724 doi: 10.1016/j.neuron.2013.03.003

725 Rodriguez, E., George, N., Lachaux, J. P., Martinerie, J., Renault, B., & Varela, F. J. (1999). Perception's
726 shadow: Long-distance synchronization of human brain activity. *Nature*, 397, 430–433. doi: 10.1038/
727 17120

728 Rolls, E. T., Huang, C. C., Lin, C. P., Feng, J., & Joliot, M. (2020). Automated anatomical labelling atlas 3.
729 *NeuroImage*, 206, 116189. doi: 10.1016/j.neuroimage.2019.116189

730 Schadow, J., Lenz, D., Thaerig, S., Busch, N. A., Fründ, I., Rieger, J. W., & Herrmann, C. S. (2007). Stim-
731 ulus intensity affects early sensory processing: Visual contrast modulates evoked gamma-band activity
732 in human EEG. *International Journal of Psychophysiology*, 66, 28–36. doi: 10.1016/j.ijpsycho.2007.05
733 .010

734 Schwab, K., Ligges, C., Jungmann, T., Hilgenfeld, B., Haueisen, J., & Witte, H. (2006). Alpha entrainment
735 in human electroencephalogram and magnetoencephalogram recordings. *NeuroReport*, 17, 1829–1833.
736 doi: 10.1097/01.wnr.0000246326.89308.ec

737 Sharpee, T. O., Sugihara, H., Kurgansky, A. V., Rebrik, S. P., Stryker, M. P., & Miller, K. D. (2006).
738 Adaptive filtering enhances information transmission in visual cortex. *Nature*, 439, 936–942. doi: 10
739 .1038/nature04519

740 Singer, W. (1999). Neuronal synchrony: A versatile code for the definition of relations? *Neuron*, 24, 49–65.
741 doi: 10.1016/S0896-6273(00)80821-1

742 Singer, W. (2009). Distributed processing and temporal codes in neuronal networks. *Cognitive Neurody-*
743 *namics*, 3, 189–196. doi: 10.1007/s11571-009-9087-z

744 Singer, W., & Gray, C. M. (1995). Visual feature integration and the temporal correlation hypothesis. *Annual*
745 *Review of Neuroscience*, 18, 555–586. doi: 10.1146/annurev.ne.18.030195.003011

746 Spaak, E., Bonnefond, M., Maier, A., Leopold, D. A., & Jensen, O. (2012). Layer-specific entrainment of
747 gamma-band neural activity by the alpha rhythm in monkey visual cortex. *Current Biology*, 22, 2313–
748 2318. doi: 10.1016/j.cub.2012.10.020

749 Spaak, E., de Lange, F. P., & Jensen, O. (2014). Local entrainment of alpha oscillations by vi-
750 sual stimuli causes cyclic modulation of perception. *Journal of Neuroscience*, 34, 3536–3544. doi:
751 10.1523/JNEUROSCI.4385-13.2014

752 Stenroos, M., Hunold, A., Eichardt, R., & Haueisen, J. (2012). Comparison of three- and single-shell
753 volume conductor models in magnetoencephalography. *Biomedizinische Technik*, 57, 311. doi: 10.1515/
754 bmt-2012-4396

755 Tallon, C., Bertrand, O., Bouchet, P., & Pernier, J. (1995). Gamma-range Activity Evoked by Coherent
756 Visual Stimuli in Humans. *European Journal of Neuroscience*, 7, 1285–1291. doi: 10.1111/j.1460-9568
757 .1995.tb01118.x

758 Tallon-Baudry, C. (2009). The roles of gamma-band oscillatory synchrony in human visual cognition.
759 *Frontiers in Bioscience*, 14, 321–332. doi: 10.2741/3246

760 Tan, H. R., Gross, J., & Uhlhaas, P. J. (2016). MEG sensor and source measures of visually induced gamma-
761 band oscillations are highly reliable. *NeuroImage*, 137, 34–44. doi: 10.1016/j.neuroimage.2016.05.006

762 Tass, P., Rosenblum, M. G., Weule, J., Kurths, J., Pikovsky, A., Volkmann, J., ... Freund, H. J. (1998).
763 Detection of n:m phase locking from noisy data: Application to magnetoencephalography. , 81, 3291–
764 3294. doi: 10.1103/PhysRevLett.81.3291

765 Traub, R. D., & Whittington, M. (2010). *Cortical Oscillations in Health and Disease*. USA: Oxford
766 University Press. doi: 10.1093/acprof:oso/9780195342796.001.0001

767 Traub, R. D., Whittington, M. A., Stanford, I. M., & Jefferys, J. G. (1996). A mechanism for generation of
768 long-range synchronous fast oscillations in the cortex. *Nature*, 383, 621–624. doi: 10.1038/383621a0

769 Uhlhaas, P. J., Pipa, G., Lima, B., Melloni, L., Neuenschwander, S., Nikolić, D., & Singer, W. (2009).
770 Neural synchrony in cortical networks: History, concept and current status. *Frontiers in Integrative*
771 *Neuroscience*, 3, 17. doi: 10.3389/neuro.07.017.2009

772 Uhlhaas, P. J., & Singer, W. (2006). Neural synchrony in brain disorders: relevance for cognitive dysfunc-
773 tions and pathophysiology. *Neuron*, 52(1), 155–168.

774 Van Pelt, S., & Fries, P. (2013). Visual stimulus eccentricity affects human gamma peak frequency. *Neu-*
775 *roImage*, 78, 439–447. doi: 10.1016/j.neuroimage.2013.04.040

776 Varela, F., Lachaux, J. P., Rodriguez, E., & Martinerie, J. (2001). The brainweb: Phase synchronization and
777 large-scale integration. *Nature Reviews Neuroscience*, 2, 229–239. doi: 10.1038/35067550

778 Veen, B., Joseph, J., & Hecox, K. (1992). Localization of intra-cerebral sources of electrical activity
779 via linearly constrained minimum variance spatial filtering. *1992 IEEE 6th SP Workshop on Statistical*
780 *Signal and Array Processing, SSAP 1992 - Conference Proceedings*, 44, 526–529. doi: 10.1109/SSAP
781 .1992.246899

782 Von der Malsburg, C. (1999). The what and why of binding: the modeler's perspective. *Neuron*, 24,
783 95–104.

784 Wehr, M., & Laurent, G. (1996). Odour encoding by temporal sequences of firing in oscillating neural
785 assemblies. *Nature*, 384, 162–166. doi: 10.1038/384162a0

786 Williams, P. E., Mechler, F., Gordon, J., Shapley, R., & Hawken, M. J. (2004). Erratum: Entrainment to
787 video displays in primary visual cortex of macaque and humans. *Journal of Neuroscience*, 24, 8278–
788 8288.

789 Womelsdorf, T., Fries, P., Mitra, P. P., & Desimone, R. (2006). Gamma-band synchronization in visual
790 cortex predicts speed of change detection. *Nature*, 439, 733–736. doi: 10.1038/nature04258

791 Xing, D., Yeh, C. I., Burns, S., & Shapley, R. M. (2012). Laminar analysis of visually evoked activity in the
792 primary visual cortex. *Proceedings of the National Academy of Sciences of the United States of America*,
793 109, 13871–13876. doi: 10.1073/pnas.1201478109

794 Zaehle, T., Rach, S., & Herrmann, C. S. (2010). Transcranial Alternating Current Stimulation Enhances
795 Individual Alpha Activity in Human EEG. *PLoS ONE*, 5, e13766. doi: 10.1371/journal.pone.0013766

796 Zhigalov, A., Herring, J. D., Herpers, J., Bergmann, T. O., & Jensen, O. (2019). Probing cortical excitability
797 using rapid frequency tagging. *NeuroImage*, 195, 59–66. doi: 10.1016/j.neuroimage.2019.03.056